8-11-2009

Energy dissipation and ion heating at the heliospheric termination shock

P. Wu

D. Winske

S. P. Gary

Nathan A. Schwadron
University of New Hampshire, Nathan.Schwadron@unh.edu

Martin A. Lee
University of New Hampshire, marty.lee@unh.edu

Energy dissipation and ion heating at the heliospheric termination shock

P. Wu,[1,2] D. Winske,[1] S. P. Gary,[1] N. A. Schwadron,[2] and M. A. Lee[3]

Received 19 March 2009; revised 26 May 2009; accepted 1 June 2009; published 11 August 2009.

[1] The Los Alamos hybrid simulation code is used to examine heating and the partition of dissipation energy at the perpendicular heliospheric termination shock in the presence of pickup ions. The simulations are one-dimensional in space but three-dimensional in field and velocity components, and are carried out for a range of values of pickup ion relative density. Results from the simulations show that because the solar wind ions are relatively cold upstream, the temperature of these ions is raised by a relatively larger factor than the temperature of the pickup ions. An analytic model for energy partition is developed on the basis of the Rankine-Hugoniot relations and a polytropic energy equation. The polytropic index γ used in the Rankine-Hugoniot relations is varied to improve agreement between the model and the simulations concerning the fraction of downstream heating in the pickup ions as well as the compression ratio at the shock. When the pickup ion density is less than 20%, the polytropic index is about 5/3, whereas for pickup ion densities greater than 20%, the polytropic index tends toward 2.2, suggesting a fundamental change in the character of the shock, as seen in the simulations, when the pickup ion density is large. The model and the simulations both indicate for the upstream parameters chosen for Voyager 2 conditions that the pickup ion density is about 25% and the pickup ions gain the larger share (approximately 90%) of the downstream thermal pressure, consistent with Voyager 2 observations near the shock.

Citation: Wu, P., D. Winske, S. P. Gary, N. A. Schwadron, and M. A. Lee (2009), Energy dissipation and ion heating at the heliospheric termination shock, *J. Geophys. Res.*, *114*, A08103, doi:10.1029/2009JA014240.

1. Introduction

[2] The heliospheric termination shock marks the heliospheric boundary where the solar wind makes the transition from a supersonic flow to a subsonic flow. It is believed to be quasi-perpendicular at most heliospheric latitudes because of the shock's great distance from the Sun and the Parker spiral structure of the heliospheric magnetic field.

[3] Voyager 1 (V1) crossed the termination shock in December 2004 at the heliocentric distance of 94 AU and a heliospheric latitude of 34.1° [*Stone et al.*, 2005]. In August 2007 Voyager 2 (V2) crossed the termination shock at 84 AU and a heliographic latitude of −27.5° [*Decker et al.*, 2008]. At the times of their respective crossings, both Voyager 1 and Voyager 2 carried operating magnetometers, but only Voyager 2 carried a functional plasma instrument. However, neither Voyager was able to measure the suprathermal ions, so there are no direct observations about the partition of dissipation energy at the termination shock.

[4] Upstream of the termination shock, ions primarily consist of protons of two distinct components: the thermal solar wind protons with a temperature T $\sim$ 1 eV and the pickup protons with an effective temperature T $\sim$ 1 keV [e.g., *Vasyliunas and Siscoe*, 1976; *Fisk and Gloeckler*, 2006]. Downstream of the shock, it was found from the Voyager 2 measurements that solar wind ions can account for only about 15% of the dissipation at the termination shock [*Richardson et al.*, 2008]. *Richardson* [2008] postulated that pickup ions account for most of the dissipation.

[5] Various analytical models and computational simulations have reached different conclusions on the partition of dissipation energy between the solar wind ions and the pickup ions, as well as the mechanism for pickup ion energization. *Zank et al.* [1996] and *Lee et al.* [1996] independently proposed that pickup ions gain a large amount of energy through repeated reflections from a very thin (electron Debye length scale) cross shock potential layer. With a one-dimensional hybrid kinetic simulation that includes electron inertia terms, *Lipatov and Zank* [1999] demonstrated that pickup ions can gain more energy than the solar wind ions through multiple reflections. However, earlier *Liewer et al.* [1993] reported that even with a 20% pickup ion relative density, their one-dimensional hybrid simulations showed that solar wind ions provide most of the termination shock dissipation. They also found that "pickup ions lead to the formation of an extended foot in front of the shock ramp of length approximately the gyroradius of the

[1]Space Science and Applications (ISR-1), Los Alamos National Laboratory, Los Alamos, New Mexico, USA.
[2]Department of Astronomy, Boston University, Boston, Massachusetts, USA.
[3]Department of Physics, University of New Hampshire, Durham, New Hampshire, USA.

0148-0227/09/2009JA014240

Table 1. Voyager 1 (V1) and Voyager 2 (V2) Termination Shock Encounters[a]

Encounters	$r(AU)$	r_S	u_u (km/s)	u_d (km/s)	θ_{Bn}	w_s (km)	τ	T_d (k)
V1	94	$2.6^{+0.4}_{-0.2}$	200	100	–	–	–	–
V2 (TS-2)	84	2.38 ± 0.14	325	150	82.8° ± 3.9°	300,300	10	10^5
V2 (TS-3)	84	1.58 ± 0.71	321	150	74.3° ± 11.2°	100,000	10	10^5

[a]TS-2 is the 2nd termination shock crossing when the termination shock is moving outward, and TS-3 is the 3rd termination shock crossing when the termination shock is moving inward. The quantity w_s is the shock width and the quantity $\tau = \frac{T_d}{T_u}$ is the temperature jump [*Richardson et al.*, 2008; *Stone et al.*, 2005; *Decker et al.*, 2005; *Burlaga et al.*, 2005; *Li et al.*, 2008].

energetic pickup ion'' [*Liewer et al.*, 1993, p. 15,219]. The fundamental difference between the *Lipatov and Zank* [1999] simulations and the *Liewer et al.* [1993] simulations is the length scale of the shock ramp where pickup ions are most likely to be accelerated.

[6] We argue that the ramp of the termination shock scales as the ion inertial length, not the electron inertial length. On the basis of early ISEE observations on strong shocks such as the Earth's bow shock, *Scudder et al.* [1986] showed that the thickness of such a shock ramp is some fraction of the upstream proton inertial length, that is, roughly the ion gyroradius. More recently, *Bale et al.* [2005] showed similar ramp thicknesses based on Cluster observations. Our simulations with zero percent pickup ions are consistent with these observations. Intuitively, we expect that with the adding of pickup ions at the termination shock, the shock will weaken and the ramp should widen. More directly, *Burlaga et al.* [2008] reported a Voyager 2 observed ramp size of one ion inertial length. Therefore the hybrid simulation (the same model *Liewer et al.* [1993] used) is still a valid tool to examine the termination shock. Our study utilizes the Los Alamos hybrid simulation code to model the relative heating of the solar wind and pickup ions at termination shocks. Our simulation has fundamentally the same physics as the *Liewer et al.* [1993] simulation. However, we apply a more accurate set of input parameters (e.g., solar wind beta and pickup ion beta) derived from the recent Voyager observations.

[7] Consider a quasi-perpendicular shock with a single, relatively cold, upstream ion component. In such shocks above the critical Mach number M_c [*Woods*, 1969], ion reflection is a well known phenomena confirmed by hybrid simulations [e.g., *Quest*, 1985; *Gosling and Robson*, 1985; *Goodrich*, 1985], laboratory studies [e.g., *Phillips and Robson*, 1972] and spacecraft observations of Earth's bow shock [e.g., *Paschmann et al.*, 1982; *Sckopke et al.*, 1983]. Adiabatic heating and anomalous resistivity are not sufficient to account for energy dissipation across such high-Mach shocks [e.g., *Kennel et al.*, 1985]. To provide additional dissipation, some ions are reflected back upstream by the shock. Those reflected ions are heated by the conversion of some of their ram energy into the energy of ion gyration. They are then convected downstream. Because the ion reflection process is nearly specular [*Gosling and Robson*, 1985], the gyrovelocities of reflected ions approximate the upstream bulk speed [*Burgess*, 1995; *Gosling and Robson*, 1985], which in this case is the upstream solar wind speed.

[8] The presence of a substantial number of pickup ions at large heliospheric distances suggests that the environment of the termination shock is very different from that of the terrestrial bow shock. The processes by which the relatively energetic pickup ions gain energy at a shock are fundamentally different from the reflection of the relatively cold solar wind ions. Using both observations and results of our hybrid simulations, this paper describes a quantitative analysis of the solar wind and the pickup ion energization at the perpendicular termination shock. Results are characterized as functions of the pickup ion relative density, ϕ, which is defined as the upstream pickup ion number density over the total upstream number density, n_u^{PUI}/n_u. Here ''PUI'' denotes pickup ion. Another puzzle in the Voyager 2 observations is that the downstream flow remains supersonic with respect to the thermal ions [*Li et al.*, 2008]. We will address this issue with our analytic model as well.

[9] Throughout this paper, r_S denotes the shock strength (or compression ratio), defined by the density jump n_d/n_u (downstream density over upstream density). The subscript ''u'' represents upstream and the subscript ''d'' represents downstream. A summary of the Voyagers' termination shock crossings is listed in Table 1 for later comparison. In the table, w_s is the shock width, which is a few times the ion inertial length and is much larger than the electron inertial length and the ion thermal gyroradius [*Richardson et al.*, 2008]. The quantities u_u and u_d are the bulk velocities upstream and downstream, respectively. The quantity θ_{Bn} is the angle between the shock normal and the local magnetic field, which is directly available from Voyager 2. The quantity T_d is the downstream temperature of the core solar wind ions. The temperature jump of these core solar wind is expressed as $\tau = T_d/T_u$. Both Voyager 1 and Voyager 2 observations show that the termination shock is a weak shock with a shock strength of about 1.6–2.6 at the locations where the Voyagers crossed it (i.e., near the nose). In this paper, we model the termination shock in a generic sense, rather than trying to reproduce explicit features of any of the Voyager shock crossings. As such, we are concerned about the ''average'' fraction of energy gain by the pickup ions at the shock (∼85%) and the ''average'' shock strength (∼2).

2. Hybrid Plasma Simulations

[10] The Los Alamos Hybrid Plasma Simulation code assumes kinetic ions and massless quasi-neutral fluid electrons [*Winske et al.*, 2003]. The code is ideal for computing ion responses to plasma phenomena (such as the termination shock) at ion inertial length and timescales. The hybrid code computes the evolution of the plasma quantities as coupled to Maxwell's equations and solves Maxwell's equations in the low-frequency limit. More details about the algorithm can be found in the work of *Winske and Omidi* [1993].

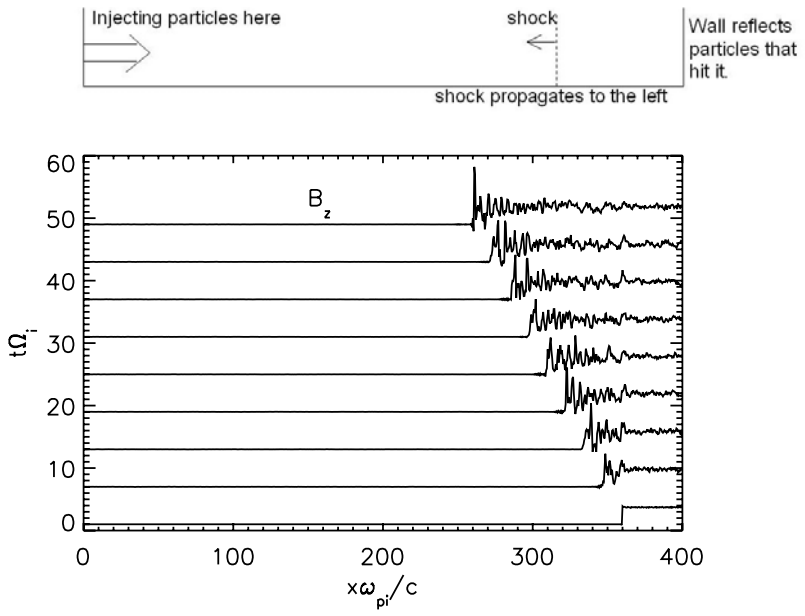

Figure 1. (top) Representative setup of a one-dimensional simulation for the termination shock. (bottom) Time evolution of the magnetic field B_z profile from a 0% pickup ion simulation. Since the simulation is run in the downstream rest frame, the shock propagates to the left. In the bottom, x is normalized by $c/\omega_{\rm pi}$ where $\omega_{\rm pi}$ is the ion plasma frequency and time t is normalized by $\Omega_{\rm i}$ where $\Omega_{\rm i}$ is the ion gyrofrequency based on the upstream magnetic field.

[11] Figure 1 (top) illustrates the one-dimensional setup for our termination shock simulations. The simulations are run in the downstream rest frame where the stationary shock propagates to the left. Except where specified, the plots in this paper are all shown in the downstream rest frame. The particles are injected from the left wall with velocity $(u_{\rm u} - u_{\rm d})$, where $u_{\rm d}$ is the downstream velocity in the shock frame calculated from the Rankine-Hugoniot relations. For the right boundary, we have included a narrow region of heated plasma with plasma conditions determined by the Rankine-Hugoniot relations. This helps to initiate the shock correctly. The boundary condition at the right wall (downstream) is then set to reflect particles that hit it. Although the simulations are one-dimensional in space, the ion velocities, fluid velocities and electromagnetic fields are fully three-dimensional.

[12] The length of the system is $400\omega_{\rm pi}/c$, where $\omega_{\rm pi}$ is the plasma frequency of the ions. The system is divided into 800 cells and the initial number of particles is 80,000 (about 100 particles per cell) for each ion component. The resistivity is set to a small value: $2 \times 10^{-5}(4\pi/\omega_{\rm pi})$. We assume that all ions are protons, and that the shock is perpendicular with the shock normal $\theta_{\rm Bn} = 90°$. The upstream parameters are chosen to be consistent with the Voyager 2 observations. Here: plasma beta $\beta_{\rm sw} = 0.05$, $u_{\rm u} = 8v_{\rm A}$ (or equivalently $M_{\rm A} = 8$) in the shock frame. The solar wind's thermal velocity distribution is assumed to be Maxwellian. We vary the pickup ion relative density from 0% to 40% to study different scenarios. The upstream pickup ion velocity distribution is assumed to be a spherical shell with the shell radius equal to the upstream bulk speed $u_{\rm u}$ because of the pickup process. Our choice of a shell distribution allows us to distinguish more clearly between the pickup ion response and the solar wind ion response to the shock. Further studies will be needed that model the upstream pickup ions using the *Vasyliunas and Siscoe* [1976] formula, which corresponds to a filled-in shell velocity distribution. Further, in this study we only consider the conditions near the shock. We do not simulate the foreshock region which extends about 10–15 AU upstream of the shock, nor do we extend our simulations deep into the downstream heliosheath.

2.1. Phase Space Density

[13] The 0% pickup ion simulation is a baseline computation that provides a comparison against the more realistic simulations (with pickup ions) to follow. Figure 1 (bottom) shows spatial profiles of the magnetic field B_z from the 0% pickup ion simulation at constant time intervals, stacked with the $t = 0$ profile on the bottom, extending to the $t = 48\ \Omega_i^{-1}$ profile on the top. Here Ω_i is the ion gyrofrequency based on the upstream magnetic field. This plot demonstrates a well-formed shock propagating to the left at a nearly constant speed, $u_{\rm sh} = -1.98v_{\rm A}$. The speed of the solar wind relative to the shock is $u_{\rm u} - u_{\rm d} + u_{\rm sh} \simeq 8v_{\rm A}$.

[14] Figure 2 shows the spatial profiles of the magnetic field and the ion density at $t = 48\Omega_i^{-1}$ from Figure 1 in more detail. The density and magnetic field profiles are similar, as expected for a perpendicular shock. The shock jump is clearly evident at $x = 259c/\omega_{\rm pi}$. In Figure 2, the ion density $n_{\rm i}$ is normalized by the upstream ion density $n_{\rm u}$; the magnetic field B_z is normalized by the upstream magnetic field B_u; and x is normalized by $c/\omega_{\rm pi}$. The upstream values are nearly constant, and the downstream average values of the density and magnetic field are ~4. The density and magnetic field jumps, as well as the amount of downstream heating, are consistent (to within ~5%) of the values based on the Rankine-Hugoniot relations [*Burgess*, 1995]. In addition, there is a large peak in both quantities at the

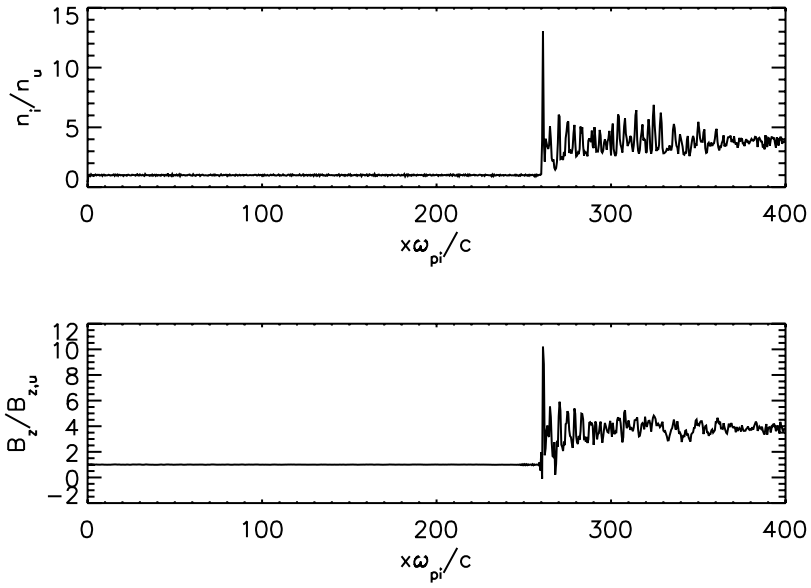

Figure 2. (top) Density profile and (bottom) magnetic field profile from a 0% pickup ion simulation. The ion density n_i is normalized by the upstream ion density n_u, the magnetic field B_z is normalized by the upstream magnetic field B_u, and x is normalized by c/ω_{pi}.

shock jump; the peaks are much higher than the average downstream values and are usually referred to as the overshoot. Downstream there are quasi-periodic oscillations around the average values. The other transverse component of the magnetic field, B_y, is about a factor of 10^3 smaller, as one would expect for a near-perpendicular shock and is not displayed.

[15] Figure 3 shows a series of phase space density plots from the simulation with pickup ion relative density $\phi = 0$. The shock is marked by a dashed line in Figures 3a and 3b. In the simulation, we identify reflected solar wind ions as the particles that are streaming upstream ($v_x < -0.4u_u$ and $v_y > 0.4u_u$) within a finite distance ($2c/\omega_{pi}$) of the shock center. The limitation is that this method cannot separate reflected ions from transmitted ions unambiguously. Because the transmitted ions can also gyrate back, a backward motion inside the shock is caused by gyration or reflection. Nevertheless, this method provides a qualitative picture of ion reflection. The transmitted solar wind ions are shown in Figure 3a, and the reflected solar wind ions are shown in Figure 3b. The plots of $v_x - x$ and $v_y - x$ indicate that the gyrophases of reflected ions are $\sim 180^\circ$ off those of the transmitted solar wind ions. Further, the gyrovelocities of the reflected ions approximate the upstream bulk velocity in the shock frame. The $v_z - z$ plots show that there is no heating in the z-direction for both the transmitted and reflected solar wind ions, a consequence of the one-dimensional perpendicular shock. The upstream solar wind ions (Figure 3c) form a Maxwellian distribution as assumed. The velocity (v_x) distributions of the downstream ions (Figure 3d) are divided into two populations: a heated transmitted population (Figure 3e) and a suprathermal tail formed by the reflected ions (Figure 3f). Both downstream populations are gyrotropic.

[16] Figure 4 presents the phase space density of both the solar wind ions and the pickup ions for the 0% pickup ion simulation. The pickup ions are test particles here; they are subject to the electromagnetic field as usual, but they make no contribution to the source terms such as density and currents. In Figure 4, solar wind ions are plotted on the left: Figures 4a and 4c (upstream), and Figure 4d (downstream). Pickup ions are plotted on the right: Figures 4b and 4e (upstream), and Figure 4f (downstream). Figures 4a and 4b (top) display the same magnetic field profile B_z. These profiles are plotted on top of both the solar wind ion images and the pickup ion images so that we can compare the scale length of B_z with the scale lengths of both populations. As Figure 4f illustrates, some pickup ions are energized and form a ring distribution. However, the average heating of the pickup ions as implied by the velocity jump, is much weaker than that of the solar wind ions. In Figure 4b, the energized pickup ions upstream of the shock form an extended region in the $v_x - x$ and the $v_y - x$ spaces (middle and bottom) as marked by two vertical grey lines. However, as test particles, pickup ions do not affect the foot of the magnetic profile (top of Figure 4b). This is not the case for our other simulations where pickup ions modify the shock profiles.

[17] Figure 5 presents the same plot as Figure 4 for the 20% pickup ion simulation. In this simulation, the shock is much weaker, with $r_S \sim 2.5$. There is a broader foot in front of the shock front in the B_z profiles, which is roughly equal to the width ($\sim 8\ \omega_{pi}/c$) of the particular pickup ion gyroradius from the shock front back into the upstream. This wider shock foot, which is caused by the presence of pickup ions in front of the shock, is marked by the two vertical grey lines in 5b. Recall that in Figure 4b (top) (the 0% pickup ion simulation), the foot is much shorter and not as visible. This difference between the 20% and the 0% pickup ion simulation is consistent with the finding of *Liewer et al.* [1993] that the foot of the shock is determined by the energized pickup ion upstream gyroradius.

[18] Figure 5a also shows that for the 20% pickup ion simulation, solar wind ions are less energized than the solar

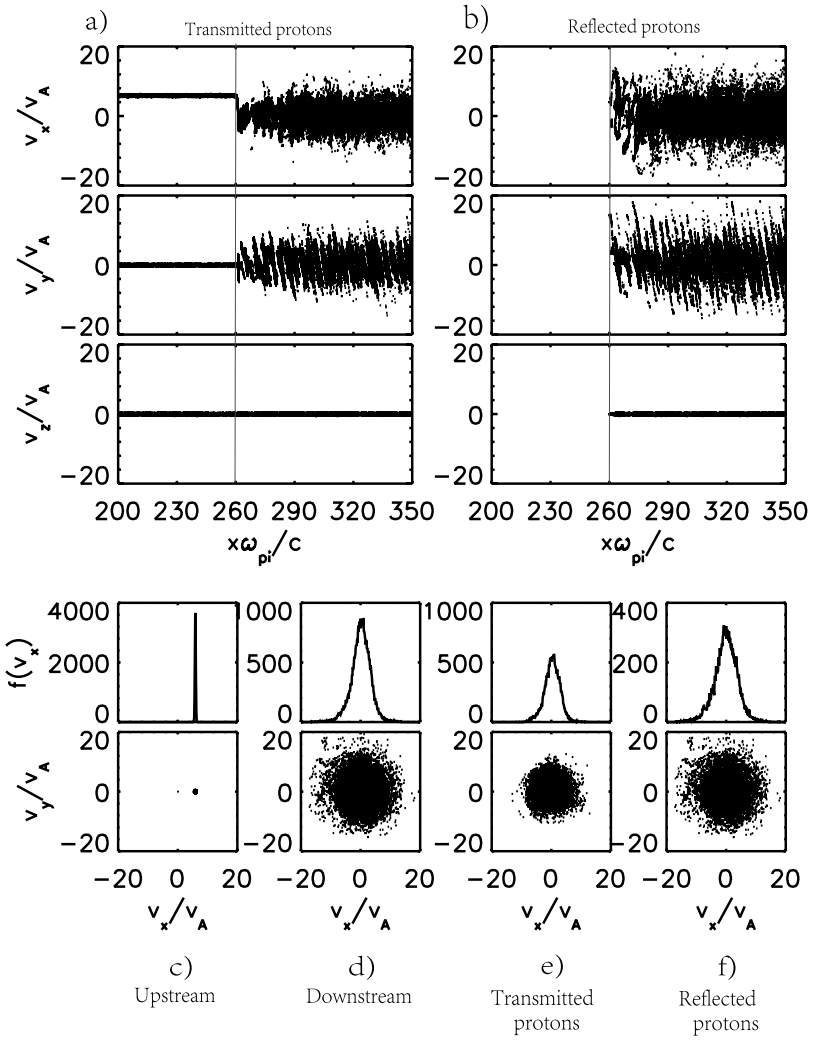

Figure 3. Phase space densities of solar wind ions in the 0% pickup ion simulation. The top are the $v_x - x$, $v_y - x$, and $v_z - x$ plots for (a) transmitted solar wind ions and (b) reflected solar wind ions. The bottom are v_x velocity distributions and $v_x - v_y$ phase space plots for (c) upstream solar wind ions, (d) downstream solar wind ions, (e) downstream transmitted solar wind ions, and (f) downstream reflected solar wind ions. The shock is marked by a dashed line in Figures 3a and 3b. The solar wind phase space density evolves from the upstream Figure 3c into the downstream Figure 3d passing the shock. Empirically, we can separate the downstream population Figure 3d into the transmitted ions in Figure 3e and the reflected ions in Figure 3f. The velocities are all normalized by the upstream Alfvén speed v_A, and x is normalized by c/ω_{pi}.

wind ions in the 0% pickup ion simulation (Figure 4a). When the pickup ion relative density is 20%, very few solar wind ions are reflected. Assuming that the wings of the downstream solar wind distributions correspond to the more energetic reflected ions, the reflection efficiency of the solar wind in the simulation with 20% pickup ions (Figure 5d) is significantly reduced in comparison with the reflection efficiency in the 0% pickup ion (Figure 4d) simulation. The average heating of the solar wind ions, however, is still stronger than that of the pickup ions. The downstream thermal velocity of the solar wind (Figure 5d) is roughly 3–4 times its upstream velocity ((Figure 5c). As seen from Figure 5f, some pickup ions are energized to form a heated ring distribution, as in Figure 4f. The downstream pickup ions (Figure 5f) are heated only ~2 times the upstream pickup ion velocity (Figure 5e), because the shock is much weaker. More precisely quantified heating ratios will be discussed in section 2.3.

2.2. Pickup Ion Trajectories

[19] Figure 6 illustrates velocity space trajectories of pickup ions from our simulation with a pickup ion relative density of 20%. The images illustrate the temporal evolution of ions that originate from the same upstream location at the start of the simulation, with one ion per image. The start time in each is marked with an asterisk, and the color changes from black to blue, green, yellow, orange and red; the last color corresponds to late-time downstream conditions. These trajectories are characteristic of the fraction of pickup ions that gain substantial energy at the shock. The

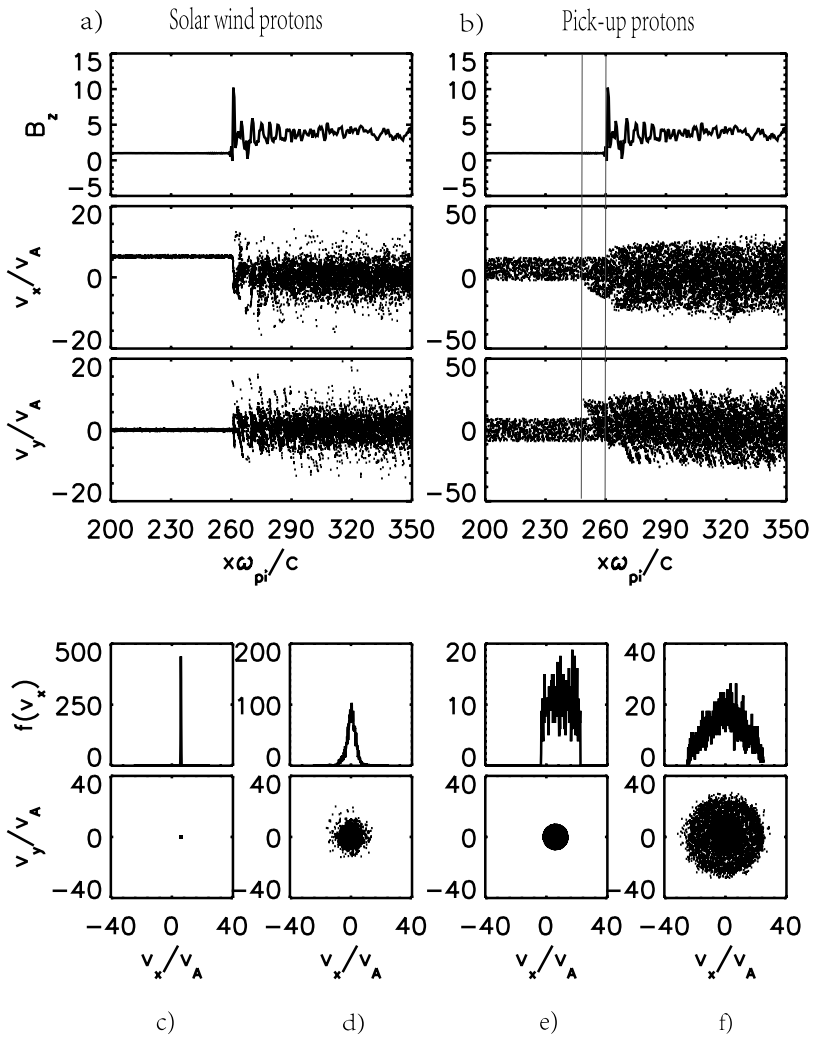

Figure 4. Phase space densities of the 0% pickup ion simulation where pickup ions are treated as test particles. Solar wind ions are plotted in Figures 4a, 4c, and 4d on the left, and pickup ions are plotted in Figures 4b, 4e, and 4f on the right. The top are magnetic field profile $B_z - x$, $v_x - x$ phase space plots, and and v_y − x phase space plots for (a) solar wind ions and (b) pickup ions. The bottom are v_x velocity distributions and $v_x - v_y$ phase space plots for (c) upstream solar wind ions, (d) downstream solar wind ions, (e) upstream pickup ions, and (f) downstream pickup ions. The velocities are all normalized by the upstream Alfvén speed v_A, and x is normalized by c/ω_{pi}.

circles with relatively large average v_x are from upstream of the shock; the transition region in green corresponds to parts of the trajectory near the shock; and the circles with relatively small average v_x are from downstream. These trajectories suggest that some pickup ions can achieve a significant energy gain at the shock, and the process involves both v_x and v_y. The mechanism by which these ions are energized will be discussed in a later publication.

2.3. Temperature Jump and Energy Partition

[20] Generally, the thermal pressure can be calculated from $P = nkT$. The temperature, T, has a dimension of energy per unit particle and represents the average kinetic energy of these particles. Pressure, P, has a dimension of energy per unit volume. We use temperature to characterize the microscopic particle energization, and pressure to describe the macroscopic partition of energy. For our simulations, the components of temperature are defined as follows

$$T_j = \frac{m_j}{3k}\left(\left\langle v_x^2 - \langle v_x\rangle^2\right\rangle + \left\langle v_y^2 - \langle v_y\rangle^2\right\rangle + \left\langle v_z^2 - \langle v_z\rangle^2\right\rangle\right). \quad (1)$$

Here the notation "$\langle\rangle$" means the average value of the enclosed parameter over all the ions of component j and over some finite spatial region within the simulation domain; m_j is the mass of ions of component j; k is the Boltzmann constant. In the one-dimensional simulation of perpendicular shocks, as shown in Figure 3, there is no heating in v_z (the velocity component parallel to the background magnetic field). Therefore it is more accurate to calculate the temperatures inferred from the simulation using only the v_x and v_y terms (velocity components perpendicular to the background magnetic field) in equation (1). Using the downstream temperatures calculated in this manner, the

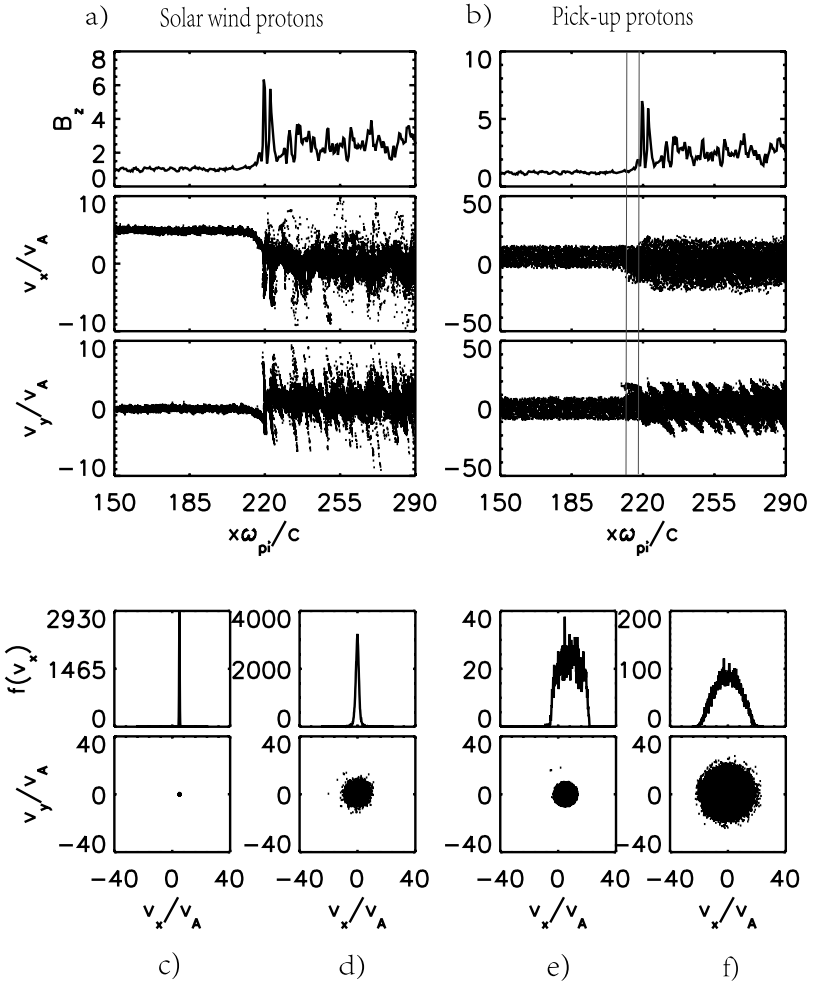

Figure 5. Phase space densities of the 20% pickup ions simulation. Solar wind ions are plotted in Figures 5a, 5c, and 5d on the left and pickup ions are plotted in Figures 5b, 5e, and 5f on the right. The top are magnetic field profile $B_z - x$, $v_x - x$ phase space plots, and $v_y - x$ phase space plots for (a) solar wind ions and (b) pickup ions. The bottom are v_x velocity distributions and $v_x - v_y$ phase space plots for (c) upstream solar wind ions, (d) downstream solar wind ions, (e) upstream pickup ions, and (f) downstream pickup ions. The velocities are all normalized by the upstream Alfvén speed v_A, and x is normalized by c/ω_{pi}.

simulated shock in the 0% pickup ion case satisfies the Rankine-Hugoniot relations.

[21] Using these temperatures computed over a spatial extent of $60c/\omega_{pi}$ upstream and downstream of the shock, we calculate the temperature jump of the solar wind ions τ_{sw} and the temperature jump of the pickup ions τ_{PUI}, both of which are listed in Table 2. In the table, n_{PUI}/n_u (input column) is the percentage of upstream pickup ions, r_S is the shock strength (compression ratio), u_d is the downstream velocity written in the unit of Alfvén speed v_A. Ideally, if all the particles are transmitted, a polytropic energy equation predicts that the temperature jump across a shock should be given by (see Appendix A for derivation)

$$\tau = \frac{T_d}{T_u} = r_S^{\gamma-1}. \tag{2}$$

In Table 2, the adiabatic temperature jump corresponding to $\gamma = 5/3$ is presented by the $\tau_{adiabat}$ column. An adiabatic transition involves no change in entropy across the shock. However, by definition, a shock is a transition across which there is an entropy increase. Because of this nonadiabatic nature of shock crossings, both the solar wind temperature jump τ_{sw} and the pickup ion temperature jump τ_{PUI} are larger than $\tau_{adiabat}$. In particular, the solar wind ions go through a much larger temperature jump than the pickup ions: $\tau_{sw} \gg \tau_{PUI} > \tau_{adiabat}$. Recall that the Rankine-Hugoniot relations determine the temperature jump across the shock, but do not indicate the nature of the heating, nor the partition of the heating if there is more than one plasma component. A polytropic law of the form of equation (2) has often been used to characterize the heating at shocks [e.g., *Feldman*, 1985], where γ becomes a parameter determined from observations. We thus define γ_{PUI} as such a parameter for characterizing pickup ion heating [*Burgess*, 1995]. The values of γ_{PUI} from our simulations can be obtained by putting the values of τ_{PUI} and r_S into equation (2), as shown in Table 2. It is shown that γ_{PUI} varies between 2.4 and 2.6 and does not depend on the pickup ion relative density. This result will be applied in section 3.

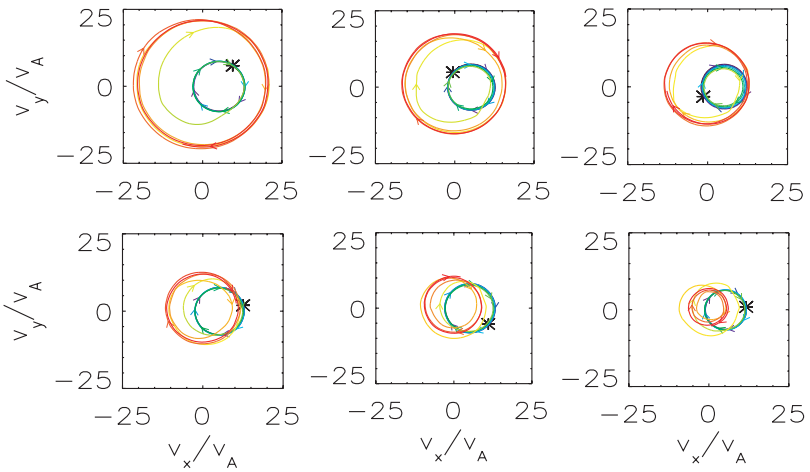

Figure 6. Pickup ion trajectories from the 20% pickup ion simulation in velocity space perpendicular to the background magnetic field. Both the v_x and v_y are normalized to the upstream Alfvén speed v_A. Each image shows a representative ion trajectory from time zero (indicated by an asterisk) to the end of the simulation. The arrows indicate the sense of temporal progress of each trajectory. From time zero, the color of each trajectory changes from black to blue, green, yellow, orange, and near the end of the simulation, to red.

[22] Compared with the observed solar wind temperature jump in Table 1, the simulated τ_{sw} values in Table 2 are larger than the observed ones. This is because the plasma instrument on Voyager 2 does not accurately measure ions in the energetic tail of the velocity distributions and therefore underestimates τ_{sw} by comparison with the simulation values.

[23] We define η_j as the percentage of thermal energy gained by each population

$$\eta_j = \frac{P_d^j V_d - P_u^i (r_S V_d)}{P_d V_d - P_u (r_S V_d)} = \frac{P_d^j - P_u^i r_S}{\sum_{i=sw,PUI} \left(P_d^i - P_u^i r_S\right)}, \quad (3)$$

where the ion component j could be the pickup ion or the solar wind ion; "sw" is short for "solar wind", V_d is the volume of the downstream ions; and so $(r_S V_d)$ is the ions' upstream volume before they cross the shock. As $P^j = n^j k T^j$, equation (3) can be rewritten as

$$\eta_j = \frac{\phi_j T_d^j - \phi_j T_u^j}{\sum_{i=sw,PUI} \left(\phi_i T_d^i - \phi_i T_u^i\right)} \quad (4)$$

for a simulation, where ϕ_j is the relative density of the ion component j. The simulation results of η_{PUI} (Table 2) show that the net energy gain of pickup ions increases with an increasing pickup ion relative density. When the pickup ion relative density is greater than 15%, pickup ions account for more than 80% of the dissipation. This is consistent with the postulation that most energy goes to pickup ions, which *Richardson et al.* [2008] drew from the Voyager 2 observations. Another way of characterizing the energy partition, for easy comparison with Voyager observations, is through the downstream thermal pressure ratio defined as

$$\chi_d = \frac{P_d^{PUI}}{P_d}. \quad (5)$$

The pressure ratio χ_d is displayed in Table 2. For the most cases, χ_d approximates η_{PUI}. Both χ_d and η_{PUI} increase as the pickup ion relative density increases. With a pickup ion ratio of 15%, χ_d is about 84%, which is the energy fraction gain for pickup ions inferred from the Voyager 2 observations by *Richardson* [2008].

3. Multicomponent Rankine-Hugoniot Model

[24] We apply the Rankine-Hugoniot jump conditions to develop a termination shock model for the partition of the downstream dissipation energy between three distinct ion

Table 2. Results Calculated from the Hybrid Simulations ($M_A = 8$, $\beta_{sw} = 0.05$)[a]

n_u^{PUI}/n_u	u_d (v_A)	$r_S = \frac{n_d}{n_u}$	$\tau_{adiabat}$	τ_{sw}	τ_{PUI}	γ_{PUI}	η_{PUI}	$\frac{P_d}{P_u}$	$\chi_d = \frac{P_d^{PUI}}{P_d}$
0%	1.98	3.87	2.47	433.64	6.91	2.43	–	1632.68	–
5%	2.27	3.22	2.18	271.24	5.86	2.51	0.42	43.32	0.46
10%	2.52	2.92	2.04	181.30	4.75	2.45	0.59	23.82	0.65
15%	2.65	2.73	1.95	88.79	4.42	2.49	0.80	15.71	0.84
20%	2.93	2.54	1.86	49.07	3.85	2.44	0.87	12.13	0.90
25%	3.36	2.33	1.75	48.85	3.43	2.45	0.87	9.97	0.90
30%	3.74	2.16	1.67	42.69	3.04	2.44	0.84	8.14	0.89
35%	3.90	2.00	1.59	35.39	2.87	2.52	0.88	7.05	0.92
40%	4.31	1.84	1.50	31.51	2.59	2.56	0.89	5.76	0.93

[a]Here energy partition $\eta_j = \frac{\phi_j T_d^j - \phi_j T_u^j}{\sum_{i=sw,PUI} \left(\phi_i T_d^i - \phi_i T_u^i\right)}$ (see section 2.3) and temperature jump $\tau_j = \frac{T_d^j}{T_u^j}$, where j denotes an ion component. The polytropic index γ_{PUI} is derived from columns τ_{PUI} and r_S using $\tau_{PUI} = r_S^{\gamma_{PUI}-1}$. In the 0% pick-up ion simulation, pick-up ions are treated as test particles.

components: transmitted solar wind ions, reflected solar wind ions, and pickup ions. We define two compression heating parameters, γ and $\gamma_{\rm PUI}$, and use them as fitting parameters to enable a comparison between the model predictions and the simulation results.

3.1. Model Equations

[25] To apply the Rankine-Hugoniot relations (Appendix A), we first need to define the upstream conditions. As noted earlier, we consider a perpendicular shock, with an upstream velocity $u_{\rm u}$ and a corresponding Alfvén Mach number $M_{\rm A} = u_{\rm u}/u_{\rm A}$, where $u_{\rm A}$ is the upstream Alfvén speed, $u_{\rm A}^2 = B_{\rm u}^2/(\mu_0\rho_{\rm u})$. We also specify the upstream solar wind temperature $T_{\rm u}^{\rm sw}$ in terms of $\beta_{\rm sw} = 2\mu_0 k T_{\rm u}^{\rm sw}\rho_{\rm u}/(m_{\rm i}B_{\rm u}^2)$. For the pickup ions, we assume a spherical shell distribution, with speed $v_{\rm shell} = u_{\rm u}$. It then follows from equation (1) that

$$P_u^{PUI} = \rho_{PUI} v_{PUI,u}^2/3 = \phi\rho_u u_u^2/3, \tag{6}$$

where ϕ is the upstream pickup ion relative density as previously defined. The pickup ions have an upstream flow velocity equal to that of the solar wind ions, $u_{\rm u}$, as implied by the pickup process. Therefore the upstream thermal pressure is given by

$$P_u = (1-\phi)P_u^{sw} + \phi P_u^{PUI} = \left[(1-\phi)\frac{\beta_{sw}}{2M_A^2} + \frac{\phi}{3}\right]\rho_u u_u^2. \tag{7}$$

It is then useful to define

$$\delta = \frac{P_u}{\rho_u u_u^2} = (1-\phi)\frac{\beta_{sw}}{2M_A^2} + \frac{\phi}{3}. \tag{8}$$

So with given upstream solar wind beta $\beta_{\rm sw}$, Alfvén Mach number $M_{\rm A}$ and heating parameters (γ, $\gamma_{\rm PUI}$), for any chosen pickup ion relative density ϕ we can calculate δ and the sonic Mach number

$$M_{cs}^2 = 1/(\gamma\delta). \tag{9}$$

Then the Rankine-Hugoniot expression (A11) (Appendix A) can be rewritten as

$$(r_S - 1)\left[r_S^2\frac{2-\gamma}{M_A^2} + r_S\left(\frac{\gamma}{M_A^2} + 2\gamma\delta + \gamma - 1\right) - (\gamma+1)\right] = 0 \tag{10}$$

and solved for $r_{\rm S}$.

[26] The Rankine-Hugoniot relations also give the downstream thermal pressure $P_{\rm d}$ in terms of the upstream pressure $P_{\rm u}$ (which we will consider shortly). However, first, we need to discuss models for the heating of the separate ion components (solar wind transmitted ions, solar wind reflected ions and pickup ions).

[27] Both the Voyager 2 observations and our hybrid simulations show that downstream pickup ions gain more energy than would be described by equation (2) with $\gamma = 5/3$. To represent this concept in our model, we assume that downstream of the shock the thermalization of the pickup ions follows a polytropic energy equation, with a $\gamma_{\rm PUI}$ to represent the amount of heating

$$P_d^{PUI} \simeq r_S^{\gamma_{PUI}} P_u^{PUI}. \tag{11}$$

Equations (6) and (11) together give

$$P_d^{PUI} = r_S^{\gamma_{PUI}}\phi\rho_u u_u^2/3. \tag{12}$$

Our simulations further show that, even with pickup ions, some solar wind ions are specularly reflected at the shock. In this model, we assume that the solar wind ions can be divided into two parts: a transmitted component and a reflected component. Let $\epsilon_{\rm ref}$ be the reflection efficiency of the solar wind ions: the number density of reflected solar wind ions divided by the number density of the solar wind ions. We assume the transmitted solar wind ions obey a polytropic energy equation, with the same γ used in equation (10) to compute the compression ratio. Then the transmitted solar wind population has a downstream pressure of

$$P_d^{sw-trans} = r_S^\gamma P_u^{sw-trans} = r_S^\gamma(1-\epsilon_{ref})P_u^{sw}, \tag{13}$$

where the superscripts "ref" and "sw-trans" represent "reflected ions" and "solar wind transmitted ions", respectively. The upstream solar wind pressure is expressed as

$$P_u^{sw} = P_u - P_u^{PUI} = P_u - \phi\rho_u u_u^2/3, \tag{14}$$

where we made use of equation (6). Equations (13) and (14) give

$$P_d^{sw-trans} = r_S^\gamma(1-\epsilon_{ref})(P_u - \phi\rho_u u_u^2/3). \tag{15}$$

For the reflected solar wind ions, because of specular reflection and subsequent energy gain in the upstream region, their downstream thermal speed is $v_{\rm d}^{\rm sw\text{-}ref} \sim u_{\rm u}$ [*Gosling and Robson*, 1985]. In fact, our 0% pickup ion simulation gives $v_{\rm d}^{\rm sw\text{-}ref} = 1.5\,u_{\rm u}$. To simplify the calculation, we adapt a value of $\sqrt{2}$ and thus we have $v_{\rm d}^{\rm sw\text{-}ref} \simeq \sqrt{2}\,u_{\rm u}$ here. We then find that

$$\begin{aligned} P_d^{sw-ref} &= \rho_d^{sw-ref}\left(v_d^{sw-ref}\right)^2/3 = (\epsilon_{ref}(1-\phi)\rho_d)2u_u^2/3 \\ &= 2r_S\epsilon_{ref}(1-\phi)\rho_u u_u^2/3. \end{aligned} \tag{16}$$

The total downstream thermal pressure can then be expressed as the sum of the transmitted solar wind thermal pressure, the reflected solar wind thermal pressure and the transmitted pickup ion thermal pressure

$$P_d = P_d^{sw-trans} + P_d^{sw-ref} + P_d^{PUI}. \tag{17}$$

Using equations (12), (15) and (16), we can rewrite the above equation as

$$\begin{aligned} P_d = {} & r_S^\gamma(1-\epsilon_{ref})(P_u - \phi\rho_u u_u^2/3) + 2r_S\epsilon_{ref}(1-\phi)\rho_u u_u^2/3 \\ & + r_S^{\gamma_{PUI}}\phi\rho_u u_u^2/3. \end{aligned} \tag{18}$$

Conservation of momentum across the shock (equation (A8)) requires that

$$\rho_u u_u^2 + P_u + \frac{B_u^2}{2\mu_0} = \rho_d u_d^2 + P_d + \frac{B_d^2}{2\mu_0}. \quad (19)$$

Substituting P_d with equation (18) and B_d with equation (A10) (Appendix A), we get

$$\rho_u u_u^2 + P_u + \frac{B_u^2}{2\mu_0} = \rho_d u_d^2 + r_S^\gamma (1-\epsilon_{ref})(P_u - \phi\rho_u u_u^2/3) + 2r_S\epsilon_{ref} \cdot (1-\phi)\rho_u u_u^2/3 + r_S^{\gamma_{PUI}}\phi\rho_u u_u^2/3 + \frac{r_S^2 B_u^2}{2\mu_0}. \quad (20)$$

Dividing equation (20) by $\rho_u u_u^2$ and solving for ϵ_{ref}, we find that

$$\epsilon_{ref} = \frac{1 - \frac{1}{r_S} + \frac{1-r_S^2}{2M_A^2} + (1-r_S)\delta + \frac{\phi}{3}\left(r_S^\gamma - r_S^{\gamma_{PUI}}\right)}{\frac{2r_S(1-\phi)}{3} + \frac{r_S^\gamma\phi}{3} - r_S^\gamma\delta}. \quad (21)$$

Since the shock strength r_S has been obtained from equation (10), we can solve for the solar wind reflection efficiency ϵ_{ref} using equation (21). In addition, the thermal pressure jump can be derived to be

$$\frac{P_d}{P_u} = r_S^\gamma(1-\epsilon_{ref})\left(1 - \frac{\phi}{3\delta}\right) + \frac{2r_S\epsilon_{ref}(1-\phi)}{3\delta} + \frac{r_S^{\gamma_{PUI}}\phi}{3\delta} \quad (22)$$

and the downstream pickup ion thermal pressure ratio (defined in section 2.3) is

$$\chi = \frac{P_d^{PUI}}{P_d} = \frac{r_S^{\gamma_{PUI}}\phi}{r_S^\gamma(1-\epsilon_{ref})(3\delta-\phi) + 2r_S\epsilon_{ref}(1-\phi) + r_S^{\gamma_{PUI}}\phi}. \quad (23)$$

In order to compare model results with Voyager observations and hybrid simulations, we choose the same input values of $M_A = 8$ and $\beta_{sw} = 0.05$, as in our simulations, for our analytic model. Table 2 shows that γ_{PUI} varies between 2.4 and 2.6 over our various simulations. Therefore we assume an average value, $\gamma_{PUI} = 2.48$, independent of the pickup ion relative density, in our analytic formula. Figure 7 then shows model results for r_S, P_d/P_u, and P_d^{PUI}/P_d as functions of the pickup ion relative density for the choice of two different values of γ: $\gamma = 5/3$ and $\gamma = 2.2$; the simulation results are indicated by the diamond symbols. Our Rankine-Hugoniot analysis shows that, for a fixed value of the pickup ion relative density, an increase in γ corresponds to a decrease in P_d/P_u (as in Figure 7, middle) and a smaller r_S (see Figure 7, top). Both the r_S and P_d^{PUI}/P_d images demonstrate that with the increase of the pickup ion relative density ϕ, the simulated values trend from the $\gamma = 5/3$ curve toward the $\gamma = 2.2$ curve. Overall, as seen from the r_S image, above 15% pickup ion relative density, a γ of 2.2 is more appropriate for characterizing the shock.

[28] The P_d^{PUI}/P_d inferred from Voyager 2 observations [*Richardson*, 2008] is approximately 85%. The values from our simulations show that, for $\phi > 15\%$, P_d^{PUI}/P_d approaches a constant value of approximately 90%, quite close to the *Richardson* [2008] value. If we combine this with the results of Figure 7 (top) and use the observed "average" Voyager 2 compression ratio of ~2, our simulations and our model with $\gamma = 2.2$ both indicate that $\phi \simeq 25\%$, which is consistent with the *Richardson* [2008] estimate.

[29] In Figure 8, ϵ_{ref} is plotted in black as a function of the pickup ion relative density ϕ. The dashed line corresponds to $\gamma = 5/3$. The reflection efficiency ϵ_{ref} in the 0% pickup ion simulation is 25% and consistent with earlier hybrid simulations [e.g., *Leroy et al.*, 1982]. The value of ϵ_{ref} drops dramatically to zero for a pickup ion relative density $\phi = 11\%$. For $\gamma = 2.2$, the reflection efficiency of solar wind ions is higher for all values of the pickup ion relative density because of the stronger heating of the pickup ions. At $\phi = 20\%$, the model predicts there is still a significant number of reflected solar wind ions, consistent with the phase space plots in Figure 5.

3.2. Energy Partition During Dissipation

[30] The percentage of thermal energy gain by the transmitted solar wind ions can be derived from equation (3)

$$\eta_{sw-trans} = \frac{(1-\epsilon_{ref})(r_S^\gamma - r_S)(\delta - \phi/3)}{\phi(r_S^{\gamma_{PUI}} - r_S)/3 + (\delta-\phi/3)\left[r_S^\gamma(1-\epsilon_{ref}) - r_S\right] + 2\epsilon_{ref}r_S(1-\phi)/3}. \quad (24)$$

Similarly, the percentages of thermal energy gain by reflected solar wind ions and pickup ions respectively are

$$\eta_{sw-ref} = \frac{2\epsilon_{ref}r_S(1-\phi)/3 - \epsilon_{ref}r_S(\delta-\phi/3)}{\phi(r_S^{\gamma_{PUI}} - r_S)/3 + (\delta-\phi/3)\left[r_S^\gamma(1-\epsilon_{ref}) - r_S\right] + 2\epsilon_{ref}r_S(1-\phi)/3}, \quad (25)$$

and

$$\eta_{PUI} = \frac{\phi(r_S^{\gamma_{PUI}} - r_S)/3}{\phi(r_S^{\gamma_{PUI}} - r_S)/3 + (\delta-\phi/3)\left[r_S^\gamma(1-\epsilon_{ref}) - r_S\right] + 2\epsilon_{ref}r_S(1-\phi)/3}. \quad (26)$$

The two quantities $\eta_{sw\text{-}ref}$ (blue) and η_{PUI} (red) are plotted in Figure 8. The dashed lines correspond to $\gamma = 5/3$, the solid line corresponds to $\gamma = 2.2$ and the simulations result are plotted as diamonds. The percentage of thermal energy gain by the reflected solar wind ions $\eta_{sw\text{-}ref}$ decreases with increasing pickup ion relative density ϕ. The percentage of thermal energy gain by the transmitted solar wind ions $\eta_{sw\text{-}trans}$ is negligibly small and is not shown. The percentage of thermal energy gain by the pickup ions η_{PUI} increases with an increasing pickup ion relative density. Above $\phi \sim 15\%$, the simulated $\eta_{PUI} \simeq$ *constant*. So at relative small values of ϕ, the simulated values are more in agreement with the Multicomponent Rankine-Hugoniot model based on a $\gamma = 5/3$ shock but they tend toward the $\gamma = 2.2$ shock solution at higher pickup ion relative densities.

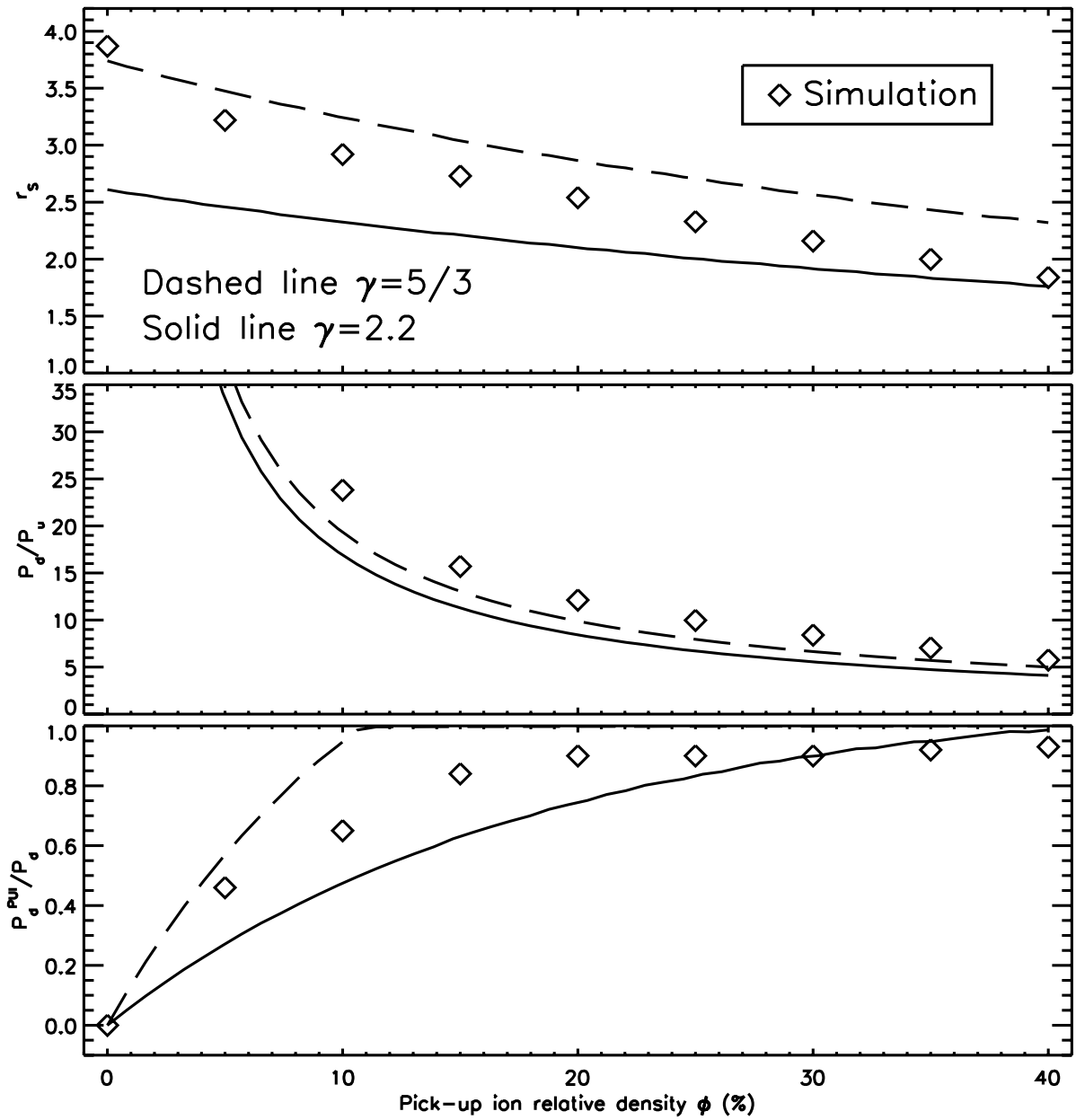

Figure 7. Compression ratio r_S, pressure jump P_d/P_u and downstream pickup ion thermal pressure ratio P_d^{PUI}/P_d as a function of the pickup ion relative density ϕ. Dashed lines are theoretical predictions when γ is set to be 5/3; the solid lines are theoretical predictions when γ is 2.2. The diamonds mark values from simulations. The horizontal lines mark Voyager 2 observed values (see section 3).

3.3. Gas Kinetic Character of the Termination Shock

[31] The downstream Alfvén Mach number can be obtained analytically with the aid of equation (A10) (Appendix A)

$$M_{A,d} = \frac{u_d}{v_{A,d}} = u_d\left(\frac{\mu_0\rho_d}{B_d^2}\right)^{1/2} = r_S^{-1.5}u_u\left(\frac{\mu_0\rho_u}{B_u^2}\right)^{1/2} = r_S^{-1.5}M_A. \tag{27}$$

With the upstream Alfvén Mach number M_A = 8 for the pickup ion relative density ϕ = [0, 40%], we calculate $M_{A,d}$ = [1.11, 2.26] (for γ = 5/3) or $M_{A,d}$ = [1.90, 3.43] (for γ = 2.2). This means that downstream of the termination shock, the flow is still super Alfvénic, which is consistent with the Voyager 2 observations [*Li et al.*, 2008].

[32] The downstream sonic Mach number can also be obtained analytically

$$M_{cs,d} = \frac{u_d}{v_{cs}} = u_d\left(\frac{\rho_d}{\gamma P_d}\right)^{1/2} = \frac{M_{cs}}{\sqrt{r_S P_d/P_u}}, \tag{28}$$

where the upstream $M_{cs} = 1/(\gamma\delta)$ as discussed previously. The pressure jump P_d/P_u is known from equation (22). For the pickup ion relative density ϕ = [0, 40%], we obtain $M_{cs,d}$ = [0.50, 0.62] (γ = 5/3) or $M_{cs,d}$ = [0.55, 0.69] (for γ = 2.2).

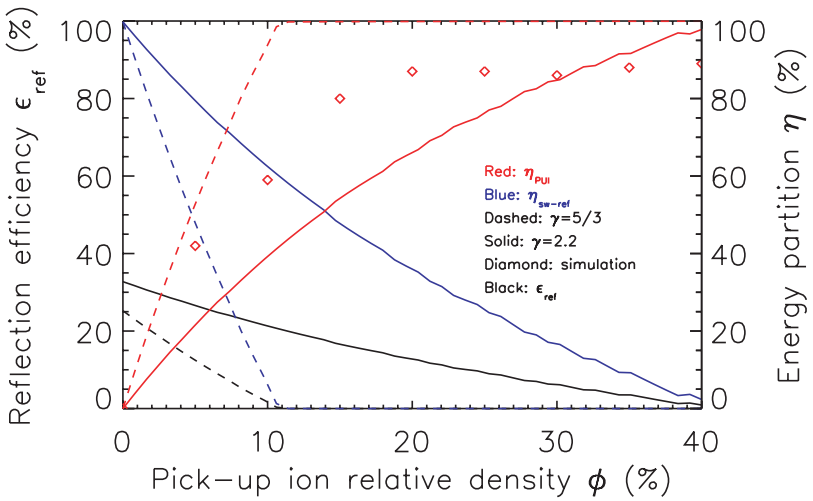

Figure 8. Solar wind reflection efficiency $\varepsilon_{\mathrm{ref}}$ (%) and termination shock energy partition η (%) as a function of the pickup ion relative density ϕ. The dashed lines correspond to $\gamma = 5/3$ and the solid lines correspond to $\gamma = 2.2$. Red diamonds mark the percentage of heating the pickup ion gain from our simulations.

[33] The magnetosonic Mach number M_{MS} [*Cravens*, 1997] is defined as the coupled Mach number of the Alfvén Mach number M_{A} and the sonic Mach number M_{cs}

$$M_{MS} = \frac{u}{\sqrt{v_A^2 + v_{cs}^2}} = \frac{M_A M_{cs}}{\sqrt{M_A^2 + M_{cs}^2}}. \tag{29}$$

For all of our simulations, the downstream magnetosonic Mach numbers fall within the range of [0.46, 0.60] (for $\gamma = 5/3$) or [0.53, 0.67] (for $\gamma = 2.2$). All the analytically calculated Mach numbers are plotted in Figure 9 as a function of ϕ. The polytropic index of $\gamma = 2.2$ predicts slightly larger downstream Mach numbers than those Mach

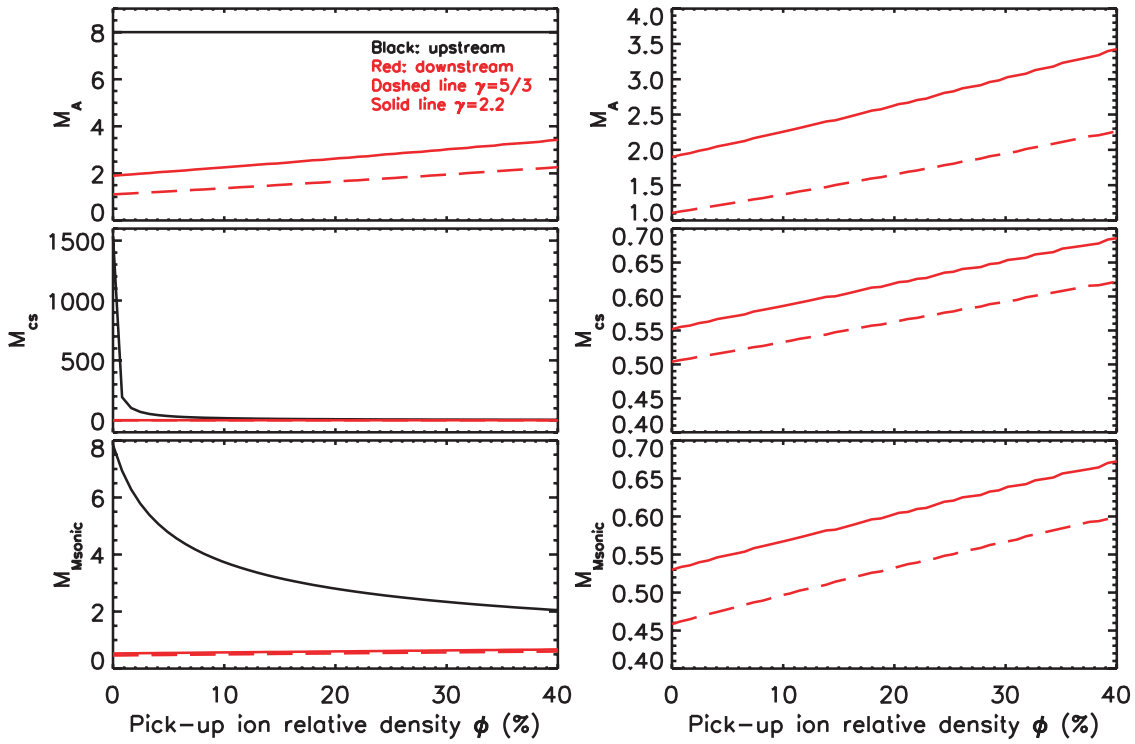

Figure 9. Mach numbers. The right images are subsets of the same quantities of the left images: (top) Alfvén Mach number M_{A}, (middle) sonic Mach number M_{cs}, (bottom) Magnetosonic Mach number M_{Msonic}. In the right, we have a better view of how the solid red lines differ from the dashed lines. The black lines are the upstream Mach numbers as a function of the pickup ion relative density ϕ; the solid red lines are the analytically calculated downstream Mach numbers at $\gamma = 2.2$, and the red dashed lines are the analytically calculated downstream Mach numbers at $\gamma = 5/3$.

numbers predicted by $\gamma = 5/3$. This is because a larger γ increases the heating, and thus lowers r_S, which results in a faster downstream flow with larger downstream Mach numbers. Although the downstream flow is super Alfvénic, it is still subsonic and submagnetosonic. The termination shock has the character resembling a gas kinetic shock as opposed to the terrestrial bow shocks, which behave as Alfvénic shocks. The participation of pickup ions in the shock dynamics causes the gas kinetic nature of the termination shock [*Fisk*, 1996].

4. Summary

[34] We have used the one-dimensional Los Alamos hybrid code to carry out a series of simulations of the perpendicular termination shock in the presence of solar wind ions and pickup ions. Our simulations show that, although the presence of the pickup ions weakens the shock, some of the upstream solar wind ions are still reflected, helping to dissipate the energy required for the shock transition. The reflected solar wind ions gain a gyrotropic speed of the order of the upstream flow speed, and are swept downstream. This process gives some solar wind ions the same order of magnitude kinetic energy as the pickup ions, so that it is difficult to observationally separate reflected solar wind ions from pickup ions downstream. The simulations also show that the termination shock is not a very strong Alfvénic shock such as the familiar terrestrial bow shock; rather, as our analytic model presents, the presence of the pickup ions raises the magnetosonic wave speed so that the termination shock behaves more like a gas kinetic shock [*Fisk*, 1996].

[35] Representative trajectories from the simulations also demonstrate that, although the pickup ion energy gain is greater than predicted by adiabatic compression, the process of specular reflection appropriate for the relatively cold solar wind ions is not applicable to the relatively warm pickup ions. Rather than a simple reversal of the radial velocity (v_x) as in reflection, both the radial and the transverse (v_y) velocity components play a role in the transfer of energy to the pickup ions.

[36] We emphasize that in this paper we have used a 1-D simulation, which precludes the excitation of downstream waves that scatter the heated solar wind and pickup ions in the direction of the magnetic field. This relaxes the downstream plasma, which in 1-D remains in a highly anisotropic state. In a future publication, we will address the impact of 2-D calculations on the amount of downstream heating and the partition of the heating between the solar wind and pickup ions.

[37] Our analytic model (Multicomponent Rankine-Hugoniot model) is based on the Rankine-Hugoniot jump conditions, a polytropic energy equation, and specular reflection for a few solar wind ions. The model computes the relative energy gain at a perpendicular shock for three proton components: transmitted solar wind ions, reflected solar wind ions, and pickup ions. Applying fitting parameters derived from our hybrid simulations to the polytropic energy equation, we can characterize the energy gains for transmitted solar wind ions and pickup ions. The reflected solar wind ion energy gain is characterized by a different parameter, which represents specular reflection, derived from the 0% pickup ion simulation. The model results are in good agreement with our simulations and are consistent with the plasma observations made by Voyager 2 at the termination shock.

[38] Our model and our simulations predict that the pickup ion relative density at the Voyager 2 crossing of the termination shock is about 25%, similar to the value of ~20% inferred from the Voyager data by *Richardson* [2008]. Comparison between the analytic results and the simulations shows that, for a pickup ion relative density larger than about 15%, the polytropic index $\gamma = 2.2$ provides a better characterization of the solar wind ion response than $\gamma = 5/3$.

[39] The simulations and the model further show that the relative energy gains of the two upstream components are sensitive functions of the relative pickup ion density. Only when the pickup ion relative density is less than ~5% does more energy go into the solar wind reflection than pickup ion heating; in this case, the solar wind component dominates the shock dissipation [*Liewer et al.*, 1993]. However, for larger pickup ion relative densities, the energy gain of pickup ions becomes much greater than that of the solar wind ions, which is the case of the termination shock. Our results support the inference by *Richardson* [2008] that most (~90%) of the dissipation is caused by pickup ions.

Appendix A

[40] For completeness, we restate the Rankine-Hugoniot jump conditions in a magnetohydrodynamic shock. The relations stated have been derived previously [e.g., *Burgess*, 1995] and are used in section 3 in the development of our multi-ion component model of the shock transition.

[41] We start with the polytropic energy equation:

$$PV^{\gamma} = constant, \tag{A1}$$

where $P = nkT \propto nkv^2$ and $V \propto 1/n$, so

$$nv^2(1/n)^{\gamma} = v^2/n^{\gamma-1} = constant. \tag{A2}$$

With upstream and downstream conditions, the above equation turns into

$$v_u^2/n_u^{\gamma-1} = v_d^2/n_d^{\gamma-1}. \tag{A3}$$

Substitute shock strength $r_S = n_d/n_u$ into equation (A3), we arrive at

$$v_d = v_u(r_S)^{(\gamma-1)/2}. \tag{A4}$$

Defining temperature jump τ

$$\tau = \frac{T_d}{T_u} = (v_d/v_u)^2 = (r_S)^{\gamma-1} \tag{A5}$$

The Rankine-Hugoniot relations for a perpendicular shock are derived in the frame of a steady shock. Both upstream and downstream plasma are assumed to satisfy the equations of ideal MHD. The resulting equations are [*Burgess*, 1995]

$$[\rho u] = 0, \tag{A6}$$

$$[uB] = 0, \tag{A7}$$

$$\left[\rho u^2 + P + \frac{B^2}{2\mu_0}\right] = 0, \tag{A8}$$

$$\left[\rho u\left(\frac{1}{2}u^2 + \frac{\gamma}{\gamma - 1}\frac{P}{\rho}\right) + u\frac{B^2}{\mu_0}\right] = 0 \tag{A9}$$

for conservation of mass, continuity of tangential electric field, conservation of momentum, and conservation of energy, respectively. In nonadiabatic situations, γ should be interpreted as the polytropic index.

[42] For a perpendicular shock

$$r_S = \frac{u_u}{u_d} = \frac{\rho_d}{\rho_u} = \frac{B_d}{B_u}. \tag{A10}$$

Combining equations (A6)–(A10), we find [*Burgess*, 1995]

$$(r_S - 1)\left[r_S^2\frac{2-\gamma}{M_A^2} + r_S\left(\frac{\gamma}{M_A^2} + \frac{2}{M_{cs}^2} + \gamma - 1\right) - (\gamma + 1)\right] = 0, \tag{A11}$$

where $M_A = u_u(\mu_0\rho_u)^{1/2}/B_u$ is the Alfvén Mach number; $M_{cs} = u_u(\rho_u/\gamma P_u)^{1/2}$ is the sonic Mach number.

[43] **Acknowledgments.** The authors thank Gary Zank, Sandra Chapman, Joe Giacalone, Herb Funsten, Jack Gosling, Chuck Goodrich, Harald Kucharek, John Richardson, and Dave McComas for helpful discussions. The Los Alamos portion of this work was performed under the auspices of the U.S. Department of Energy (DOE) and was supported by the Solar and Heliospheric Physics SR&T Program of the National Aeronautics and Space Administration (NASA). The Boston University portion is funded and supported by the NASA Intersteller Boundary Explorer (IBEX) mission, which is part of the Goddard Space Flight Center (GSFC) Explorer Program. We also acknowledge support from an NSF-SHINE grant (Dynamical Properties of Suprathermal Ions in the 3-D Heliosphere, ATM-0550905).

[44] Wolfgang Baumjohann thanks Nick Omidi for his assistance in evaluating this paper.

References

Bale, S. D., et al. (2005), Quasi-perpendicular shock structure and processes, *Space Sci. Rev.*, *118*, 161–203, doi:10.1007/s11214-005-3827-0.

Burgess, D. (1995), Collisionless shocks, in *Introduction to Space Physics*, edited by M. G. Kivelson and C. T. Russell, pp. 129–163, Cambridge Univ. Press, New York.

Burlaga, L. F., N. F. Ness, M. H. Acuna, R. P. Lepping, J. E. Connerney, E. C. Stone, and F. B. McDonald (2005), Crossing the termination shock into the heliosheath: Magnetic fields, *Science*, *309*, 2027–2029, doi:10.1126/science.1117542.

Burlaga, L. F., N. F. Ness, M. H. Acuna, R. P. Lepping, J. E. P. Connerney, and J. D. Richardson (2008), Magnetic fields at the solar wind termination shock, *Nature*, *454*, 75–77, doi:10.1038/nature07029.

Cravens, T. E. (1997), *Physics of Solar System Plasmas*, 134 pp., Cambridge Univ. Press, New York.

Decker, R. B., S. M. Krimigis, E. C. Roelof, M. E. Hill, T. P. Armstrong, G. Gloeckler, D. C. Hamilton, and L. J. Lanzerotti (2005), Voyager 1 in the foreshock, termination shock, and heliosheath, *Science*, *309*(5743), 2020–2024, doi:10.1126/science.1117569.

Decker, R. B., S. M. Krimigis, E. C. Roelof, M. E. Hill, T. P. Armstrong, G. Gloeckler, D. C. Hamilton, and L. J. Lanzerotti (2008), Mediation of the solar wind termination shock by non-thermal ions, *Nature*, *454*, 67–70, doi:10.1038/nature07030.

Feldman, W. C. (1985), Electron velocity distributions near collisionless shocks, in *Collisionless Shocks in the Heliosphere: Reviews of Current Research*, *Geophys. Monogr. Ser.*, vol. 35, edited by B. T. Tsurutani and R. G. Stone, pp. 195–205, AGU, Washington, D. C.

Fisk, L. A. (1996), Implication of a weak termination shock, in *Space Sci. Rev.*, vol. 78, edited by R. Steiger, R. Lallement, and M. Lee, pp. 129–136, doi:10.1007/BF00170799, Kluwer Acad., Netherlands.

Fisk, L. A., and G. Gloeckler (2006), The common spectrum for accelerated ions in the quiet-time solar wind, *Astrophys. J.*, *640*, *1*, L79–L82, doi:10.1086/503293.

Goodrich, C. C. (1985), Numerical simulations of quasi-perpendicular collisionless shock, in *Collisionless Shocks in the Heliosphere: Reviews of Current Research*, *Geophys. Monogr. Ser.*, vol. 35, edited by B. T. Tsurutani and R. G. Stone, pp. 153–168, AGU, Washington, D. C.

Gosling, J. T., and A. E. Robson (1985), Ion reflection, gyration, and dissipation at supercritical shocks, in *Collisionless Shocks in the Heliosphere: Reviews of Current Research*, *Geophys. Monogr. Ser.*, vol. 35, edited by B. T. Tsurutani and R. G. Stone, pp. 141–152, AGU, Washington, D. C.

Kennel, C. F., J. P. Edmiston, and T. Hada (1985), A quarter century of collisionless shock research, in *Collisionless Shocks in the Heliosphere: A Tutorial Review*, *Geophys. Monogr. Ser.*, vol. 34, edited by R. G. Stones and B. T. Tsurutani, pp. 1–36, AGU, Washington, D. C.

Lee, M. A., V. D. Shapiro, and R. Z. Sagdeev (1996), Pickup ion energization by shock surfing, *J. Geophys. Res.*, *101*(A3), 4777–4790.

Leroy, M. M., D. Winske, C. C. Goodrich, C. S. Wu, and K. Papadopoulos (1982), The structure of perpendicular bow shocks, *J. Geophys. Res.*, *87*(A7), 5081–5094.

Li, H., C. Wang, and J. D. Richardson (2008), Properties of the termination shock observed by Voyager 2, *Geophys. Res. Lett.*, *35*, L19107, doi:10.1029/2008GL034869.

Liewer, P. C., B. E. Goldstein, and N. Omidi (1993), Hybrid simulations of the effects of interstellar pickup hydrogen on the solar wind termination shock, *J. Geophys. Res.*, *98*(A9), 15,211–15,220.

Lipatov, A. S., and G. P. Zank (1999), Pickup ion acceleration at low-β_p perpendicular shocks, *Phys. Rev. Lett.*, *82*(18), 3609–3612, doi:10.1103/PhysRevLett.82.3609.

Paschmann, G., N. Sckopke, S. J. Bame, and J. T. Gosling (1982), Observations of gyrating ions in the foot of the nearly perpendicular bow shock, *Geophys. Res. Lett.*, *9*(8), 881–884.

Phillips, P. E., and A. E. Robson (1972), Influence of reflected ions on the magnetic structure of a collisionless shock front, *Phys. Rev. Lett.*, *29*(154), doi:10.1103/PhysRevLett.29.154.

Quest, K. B. (1985), Simulation of high-Mach-number collisionless perpendicular shock in astrophysical plasmas, *Phys. Rev. Lett.*, *54*(16), 1872–1874, doi:10.1103/PhysRevLett.54.1872.

Richardson, J. D. (2008), Plasma temperature distributions in the heliosheath, *Geophys. Res. Lett.*, *35*, L23104, doi:10.1029/2008GL036168.

Richardson, J. D., J. C. Kasper, C. Wang, J. W. Belcher, and A. J. Lazarus (2008), Cool heliosheath plasma and deceleration of the upstream solar wind at the termination shock, *Nature*, *454*, 63–66, doi:10.1038/nature07024.

Sckopke, N., G. Paschmann, S. J. Bame, J. T. Gosling, and C. T. Russell (1983), Evolution of ion distribution across the nearly perpendicular bow shock: Specularly and non-specularly reflected-gyrating ions, *J. Geophys. Res.*, *88*(A8), 6121–6136.

Scudder, J. D., A. Mangeney, C. Lacombe, C. C. Harvey, T. L. Aggson, R. R. Anderson, J. T. Gosling, G. Paschmann, and C. T. Russell (1986), The resolved layer of a collisionless, high β, supercritical, quasi-perpendicular shock wave: 1. Rankine-Hugoniot geometry, currents, and stationarity, *J. Geophys. Res.*, *91*(A10), 11,019–11,052.

Stone, E. C., A. C. Cummings, F. B. McDonald, B. C. Heikkila, N. Lal, and W. R. Webber (2005), Voyager 1 explores the termination shock region and the heliosheath beyond, *Science*, *309*(5743), 2017–2020, doi:10.1126/science.1117684.

Vasyliunas, V. M., and G. L. Siscoe (1976), On the flux and energy spectrum of interstellar ions in the solar system, *J. Geophys. Res.*, *81*(7), 1247–1252.

Winske, D., and N. Omidi (1993), Hybrid codes: Methods and applications, in *Computer Space Plasma Physics: Simulation Techniques and Soft-*

ware, edited by H. Matsumoto and Y. Omura, pp. 103–160, Terra Sci., Tokyo.

Winske, D., L. Yin, N. Omidi, H. Karimabadi, and K. B. Quest (2003), Hybrid simulation codes: Past, present and future—A tutorial, in *Space Plasma Simulation*, edited by J. Buechener, C. T. Dum, and M. Scholer, pp. 140–169, Springer, Germany.

Woods, L. C. (1969), Critical Alfvén mach numbers for transverse field MHD shocks, *Plasma Phys.*, *11*, 25–34, doi:10.1088/0032-1028/11/1/004.

Zank, G. P., H. L. Pauls, I. H. Cairns, and G. M. Webb (1996), Interstellar pickup ions and quasi-perpendicular shocks: Implications for the termination shock and interplanetary shocks, *J. Geophys. Res.*, *101*(A1), 457–478.

S. P. Gary and D. Winske, Space Science and Applications, Los Alamos National Laboratory, Mail Stop D466, Group ISR-1, Los Alamos, NM 87545, USA. (pgary@lanl.gov; winske@lanl.gov)

M. A. Lee, Department of Physics, University of New Hampshire, 39 College Road, Durham, NH 03824, USA.

N. A. Schwadron and P. Wu, Department of Astronomy, Boston University, 725 Commonwealth Avenue, Boston, MA 02215, USA. (nathanas@bu.edu; nanopenny@gmail.com)